Article

Performance Bound for Joint Multiple Parameter Target Estimation in Sparse Stepped-Frequency Radar: A Comparison Analysis

Qiushi Chen [1], **Xin Zhang [1,2]**, **Qiang Yang [1,2,*]**, **Lei Ye [1]** and **Mengxiao Zhao [1]**

[1] Department of Electronic and Information Engineering, Harbin Institute of Technology, Harbin 150001, China; chenqiushi@126.com (Q.C.); zhangxinhit@hit.edu.cn (X.Z.); yedaily@163.com (L.Y.); zmx_zhao@163.com (M.Z.)

[2] Key Laboratory of Marine Environmental Monitoring and Information Processing, Ministry of Industry and Information Technology, Harbin 150001, China

* Correspondence: yq@hit.edu.cn

Abstract: A performance bound—Cramér-Rao lower bound (CRLB) for target estimation and detection in sparse stepped frequency radars is presented. The vector formulation of this CRLB is used to obtain a lower bound on the estimation error. The estimation performance can be transformed into different types of CRLB structures. Therefore, the expressions of bounds under three equivalent models are derived separately: time delay and Doppler stretch estimator, joint multiple parameter estimator, and sparse-based estimator. The variables to be estimated include the variances of unknown noise, range, velocity, and the real and imaginary parts of the amplitude. A general performance expression is proposed by considering the echo of the target in the line-of-sight. When the relationship between CRLB and various parameters are discussed in detail, the specific effect of waveform parameters on a single CRLB is compared and analyzed. Numerical simulations demonstrated that the resulting CRLB exhibits considerable theoretical and practical significance for the selection of optimal waveform parameters.

Keywords: targets estimation and detection; performance analysis; sparse stepped frequency; Cramér-Rao lower bound

1. Introduction

A sparse stepped frequency (SSF) signal extends the traditional continuous bandwidth to random discontinuous frequency bands in modern radars. However, the performance of SSF signals has not been evaluated effectively. The Cramér-Rao lower bound (CRLB) expresses the lower bound of the variance of unbiased estimators in [1,2], which has a wide range of applications in radar. Various CRLBs of joint parameter estimation for broadband signals have been proposed.

In [2], a Gaussian signal and a linear frequency modulation (LFM) signal are analyzed. It is verified that the CRLB of joint estimation depends on the signal-noise-ratio (SNR), threshold, and signal structure. In [3,4], an LFM signal is used to analyze the CRLB of joint Range–Doppler(RD) estimation performance in both active radar and distributed passive radar networks. Particularly in [5], the CRLB of RD estimation is computed using FM commercial radio signals for passive radar network systems; this demonstrates that the coherent CRLB is much lower than that of the noncoherent processing mode. Subsequently, a modified CRLB is investigated in [6]; it is applicable for passive multistatic radar systems with antenna arrays. Analysis confirmed that the joint estimation performance is related to the geometry of the target, radar configuration, SNR, and signal parameters. Reference [7] investigates the CRLB of the joint target radial velocity and the acceleration estimation performance of an linear

stepped frequency (LSF) signal. In [8], the CRLB expression is derived to guide TDOA estimation using a frequency-hopping signal. Similarly, in [9,10], the performance of joint TD estimation is studied with random stepped frequency signals. In addition, some researchers have explored the performances of other parameters; e.g., in [11,12], the CRLB of a target's position, intensity, and geometry type are derived by considering the signal as a geometric theory of diffraction (GTD)-based scattering center model. The CRLBs of a known and an unknown phase for joint RD estimation is presented in [13]; the unknown time delay, Doppler stretch, amplitude, and uniform distributed initial phase are estimated simultaneously in [14]. Although the target estimation of an SSF signal has been employed in wideband radar system [15–17], the CRLB performance expression above for various waveforms cannot be applied directly to an SSF. In fact, compared with an LFM or LSF signal with limited continuous bandwidth, an SSF exhibits a higher synthetic bandwidth, thus, enabling it to improve the resolution of separating multiple close-range spatial targets. Moreover, because its carrier frequency is sparse and exhibits random hopping, the range–Doppler coupling problem can be suppressed effectively [18]; further, the interference from other users can be avoided.

The parameters of target echo, and environmental and transmit waveforms affect the performance significantly. Therefore, the relationship among these parameters and the estimation performance are compared and analyzed. Some conclusions have been drawn from the following studies. In [19], the CRB for the unbiased estimators of parameters from compressed samples are investigated. The CRB increases when the number of compressed samples is larger than that of the targets. In [20], the CRLB criterion of time delay estimation is analyzed under various pulse shapes. It is concluded that the performance depends on the pulse's period, order, and shape. In [21], the estimation performances for uniform and nonuniform frequency samplings are analyzed. The best sampling set is gained by statistical strategy. In [2], it verifies that the CRLB of the joint estimation depends on the SNR, threshold, and signal structure. In [14], the performances of unknown time delay, Doppler stretch, amplitude, and uniform distributed initial phase are explored simultaneously. In [22,23], primary factors including the SNR, central carrier frequency, carrier frequency bandwidths and frequency shifting code words that affect the performance are discussed.

These expressions effectively explain the CRLB for target estimation in previous references. However, because of the sparseness and irregularity of the selected frequencies, the existing regularity for linear frequencies is no longer applicable in the sparse signal. Therefore, a new process of performance analysis for an SSF signal is necessary. In this work, the estimation problem using an SSF signal as a transmitting waveform can be equivalent to that of the three different structures. The accordance expression of a special CRLB deduction can be obtained based on a variant SSF. All relevant variables are retained without simplification in the process to facilitate the further analysis of the parameter relationships accordingly.

The primary work and contributions can be stated as follows: First, by referring to the CRLB of delay and Doppler stretch equivalent model used in the wideband signal [2] and in random stepped frequency signal [9], a general representation of the same performance is derived by considering an SSF signal with a chirp envelope. After setting some of the parameters, the CRLBs of an SSF signal with a rectangular envelope are verified. Next, according to the GTD-based scattering center estimation [11], the similar CRLB for multiple parameter estimations using an SSF waveform is derived. The actual performances under various model assumptions are analyzed comprehensively and systematically. Subsequently, a sparse-based expression for model error [24] is substituted directly into the SSF estimation for introducing the CS estimation method. Finally, the degree and trend of each individual coefficient constituting the bound of the entire joint estimation are discussed. The relationship between the CRLB and various parameters are developed in detail. The resulting CRLB above presents instructional significance for transmitting waveform optimization.

The remainder of this paper is organized as follows. In Section 2, the signal model for the SSF signal is introduced. In Section 3, The CRLB of basic LSF and SSF signals within a time delay and Doppler stretch model are presented. In Section 4, the CRLB of joint multiple parameter estimation is

discussed. In Section 5, the CRLB of a sparse-based estimator is introduced. Numerical simulation examples and results are described in Section 6 and conclusions are presented.

Notation 1. *A capital bold letter* **x** *represents a matrix.* $x(n)$ *is the* n^{th} *sample point. A letter with superscript* $\hat{\theta}$ *represents the estimation of* θ. $E\{\cdot\}$ *represents the expectation operator.* $\text{Tr}(\cdot)$ *denotes the trace of matrix.* $\lfloor \cdot \rfloor$ *is the rounding operator.* $\|\cdot\|_0$ *represents the* ℓ_0 *norm.* $\|\cdot\|_2$ *is the standard Euclidean norm with the value* $\|x\|_2 = \sqrt{\sum_i |x_i|^2}$. *The symbol* ∂ *is the partial derivative operator.* $(\cdot)^*$, $(\cdot)^T$, *and* $(\cdot)^H$ *indicate the conjugate, transpose, and conjugate transpose.*

2. Signal Model

In this study, t_n denotes the sampling time of the nth pulse; the width of every narrow band pulse is T_w, pulse repetition interval (PRI) is T. Therefore, the transmitting signal is

$$x_0(t) = \sum_{n=0}^{N-1} \text{rect}\left(\frac{t - nT}{T_w}\right) e^{-j2\pi f_n t} \tag{1}$$

where $\text{rect}(\cdot)$ stands for a rectangular function with

$$\text{rect}\left(\frac{t}{T}\right) = \begin{cases} 1, & -T/2 \le t \le T/2 \\ 0, & \text{else} \end{cases}$$

f_n is set as the chosen frequency for every pulse. It is noteworthy that the transmitting frequencies can be calculated by $f_n = f_0 + C_n \Delta f$, where f_0 is the initial carrier frequency, and Δf is the frequency step. The sequence of frequencies is $C_n \in [1, M]$ with $N = \|\mathbf{C}\|_0 <= \|\mathbf{m}\|_0 = M$, where M is the total multiples of step Δf in the whole frequency span, and N is the number of transmitting pulses. The frequency pattern is determined by n and C_n.

The receiving signal is the time delay and Doppler stretch version of the transmitting signal. After processing by mixing and sampling, the discrete form of the echo is

$$\begin{aligned} y(n) &= x(n) + w(n) \\ &= \sum_{k=1}^{K} A_k e^{-j4\pi(f_0 + C_n \Delta f)(R_k + V_k nT)/c} + w(n) \end{aligned} \tag{2}$$

where the kth target signal consists of the range R_k, velocity V_k, and echo amplitude A_k. When $K = 1$, $x(n)$ in (2) can be simplified as

$$x(n) = A e^{-j4\pi f_n (R + VnT)/c}. \tag{3}$$

Defining $\mathbf{y} = [y(1), y(2), ..., y(n)]^T$ and $\mathbf{x} = [x(1), x(2), ..., x(n)]^T$, the matrix form is given by $\mathbf{y} = \mathbf{x} + \mathbf{w}$. $w(n)$ is the zero-mean white Gaussian noise (WGN), which is distributed as $\mathbf{w} \sim N(0, \sigma^2)$. The estimation performance for this type of signal model will be studied in the next section.

3. CRLB of Basic LSF and SSF Signals—Time Delay And Doppler Stretch

We derived a performance bound for the SSF waveform. The relationship among all the parameters is analyzed to provide useful information for waveform optimization. From this theory performance, the range–Doppler information can be estimated more efficiently in the radar system.

The receiving signal can be transferred into the time delay and Doppler stretch versions as the form in [2] from the transmitting signal, that is

$$s(t) = ax((t - \tau)/\sigma) + w(t) \tag{4}$$

where $\tau = 2R/c$ is the time delay of the echo from the target at distance R (range is proportional to time delay; therefore, we use the time delay to explain the estimation in the range domain), c is the speed of light, $\sigma = \dfrac{c+v}{c-v}$ is the Doppler stretch, a is the amplitude. Here, we define the SNR using the signal power E and power spectrum density (PSD) N_0 of $w(t)$, that is

$$E = a^2 \int_{-\infty}^{\infty} |s(t)|^2 dt. \tag{5}$$

We will consider the estimation performance for this type of signal model. The CRLBs of the joint time and Doppler estimation are derived. The probability density function(PDF) $p(s|\boldsymbol{\theta})$ of the complex echo signal x is given by

$$p(s|\boldsymbol{\theta}) = K \exp \left\{ -\frac{1}{N_0} \int_{-\infty}^{\infty} |s(t) - ax\left(\sigma\left(t-\tau\right)\right)|^2 dt \right\} \tag{6}$$

where K is a constant, and $\boldsymbol{\theta} = [\tau \ \ \sigma]$ is the parameter vector to be estimated. The covariance matrix for an unbiased estimate $\hat{\boldsymbol{\theta}}$ satisfies

$$\mathrm{CRLB}_{\hat{\boldsymbol{\theta}}} = E\left[\left(\hat{\boldsymbol{\theta}} - \boldsymbol{\theta}\right) \cdot \left(\hat{\boldsymbol{\theta}} - \boldsymbol{\theta}\right)^T\right] \geq \mathbf{J}^{-1} \tag{7}$$

where $()^T$ is the transpose of a vector, and $\mathbf{J}$ is the Fisher information matrix (FIM), which is defined by [1,2]

$$\boldsymbol{J}(\theta) = E\left\{\nabla_{\theta} \ln p(s|\boldsymbol{\theta}) \cdot [\nabla_{\theta} \ln p(s|\boldsymbol{\theta})]^T\right\} \tag{8}$$

Therefore, the FIM is

$$\mathbf{J}^{-1}(\theta) = \frac{N_0 \sigma}{2|a|^2 \left(D_s B_s - C_s^2\right)} \begin{bmatrix} D_s & -C_s \\ -C_s & B_s \end{bmatrix} \tag{9}$$

where $B_s \overset{\Delta}{=} \int_{-\infty}^{\infty} |\dot{s}(t)|^2 dt$, $C_s \overset{\Delta}{=} \int_{-\infty}^{\infty} t|\dot{s}(t)|^2 dt$, $D_s \overset{\Delta}{=} \int_{-\infty}^{\infty} t^2|\dot{s}(t)|^2 dt$, $\dot{s}(t) = ds(t)/dt$. The CRLBs of the time delay and Doppler stretch can be specifically expressed as

$$\mathrm{var}\left(\hat{\tau}\right) = \left[\mathbf{J}^{-1}(\theta)\right]_{11} = \frac{N_0 \sigma D_s}{2|a|^2 \left(D_s B_s - C_s^2\right)} \tag{10}$$

$$\mathrm{var}\left(\hat{\sigma}\right) = \left[\mathbf{J}^{-1}(\theta)\right]_{22} = \frac{N_0 \sigma B_s}{2|a|^2 \left(D_s B_s - C_s^2\right)} \tag{11}$$

3.1. CRLB of SSF-Chirp Signals

From (10) and (11), the CRLB performance of the signal waveform depends on the signal parameters B_s, C_s, and D_s. We impose SF signal (4) into them, and subsequently calculate the theoretical performances of the CRLBs. This rectangular function can be expressed in the form of a unit step function, that is

$$\int_{-\infty}^{+\infty} s(t)\left[u\left(t+\frac{T_w}{2}\right) - u\left(t-\frac{T_w}{2}\right)\right] dt = \int_{nT-\frac{T_w}{2}}^{nT+\frac{T_w}{2}} s(t) dt. \tag{12}$$

Therefore, the first power of t_n can be calculated under the interval from $\left(nT - \dfrac{T_w}{2} \right)$

to $\left(nT + \dfrac{T_w}{2} \right)$; therefore, $t_n \Big|_{nT-\frac{T_w}{2}}^{nT+\frac{T_w}{2}} = T_w$ is obtained. Similarly, the quadratic term

is $t_n^2 \Big|_{nT-\frac{T_w}{2}}^{nT+\frac{T_w}{2}} = 2nTT_w$, the third term is $t_n^3 \Big|_{nT-\frac{T_w}{2}}^{nT+\frac{T_w}{2}} = \dfrac{T_w^3}{4} + 3n^2 T_w T^2$, the forth term is

$t_n^4 \Big|_{nT-\frac{T_w}{2}}^{nT+\frac{T_w}{2}} = T_w^3 Tn + 4n^3 T_w T^3$ and the fifth term is $t_n^5 \Big|_{nT-\frac{T_w}{2}}^{nT+\frac{T_w}{2}} = \dfrac{T_w^5}{16} + \dfrac{5n^2 T_w^3 T^2}{2} + 5n^4 T_w T^4$.

To simplify the expressions above, we introduce $Z_{(i,j)} = \sum\limits_{n=0}^{N-1} n^i f_n^{\ j} (0 \le i \le 4, 0 \le j \le 2)$ into the following deviation. The parameter values of a chirp envelope are as follows:

$$
\begin{cases}
(B_s)_{chirp} = 4\pi^2 \left(\begin{array}{c} z_{(0,2)} + \gamma T z_{(1,1)} \\[4pt] + \dfrac{1}{4}\gamma^2 T^2 z_{(2,0)} + \dfrac{1}{48}\gamma^2 N T_w^2 \end{array} \right) \\[30pt]
(C_s)_{chirp} = 4\pi^2 \left(\begin{array}{c} \dfrac{\gamma T_w^2}{12} z_{(0,1)} + \dfrac{1}{16}\gamma^2 T_w^2 T z_{(1,0)} + T z_{(1,2)} \\[4pt] + \gamma T^2 z_{(2,1)} + \dfrac{1}{4}\gamma^2 T^3 z_{(3,0)} \end{array} \right) \\[30pt]
(D_s)_{chirp} = 4\pi^2 \left(\begin{array}{c} \dfrac{T_w^2}{12} Z_{(0,2)} + \dfrac{1}{4}\gamma T_w^2 T z_{(1,1)} \\[4pt] + \dfrac{\gamma^2 T_w^2 T^2}{8} z_{(2,0)} + T^2 Z_{(2,2)} \\[4pt] + \gamma T^3 z_{(3,1)} + \dfrac{\gamma^2 T^4}{4} z_{(4,0)} + \dfrac{\gamma^2 T_w^4 N}{320} \end{array} \right)
\end{cases}
\tag{13}
$$

The values of the CRLBs depend on not only the total number of pulses M, but also the selected frequencies f_n, but the frequency pattern from the relationship between sequence of pulses n and sequence of frequency C_n.

3.2. SSF-Rect Signals

When the slope with the value $\gamma = 0$, the envelope of the SSF signal changes from chirp to rectangular, namely an SSF-rect signal. Therefore, substituting $\gamma = 0$ into (13), the intermediate variables for an SSF-rect signal are

$$
\begin{cases}
(B_s)_{rect} = 4\pi^2 T_w z_{(0,2)} \\[6pt]
(C_s)_{rect} = 4\pi^2 TT_w z_{(1,2)} \\[6pt]
(D_s)_{rect} = 4\pi^2 T_w \left(T^2 z_{(2,2)} + T_w^2 z_{(0,2)}/12 \right)
\end{cases}
\tag{14}
$$

When $N = M$, $C_n = n$, the signal will be in the form of an LSF signal. The expression is the same as that of the SSF for cases involving a chirp envelope and a rectangular envelope. Similarly, when $n = 0$, $N = 1$, $f_n = f$, SSF signal will degenerate into LFM signal. We obtain $z_{(0,1)} = f_0$, other values in $z_{(i,j)}$ are equal to 0.

4. CRLB of Joint Multiple Parameter Estimation

4.1. Basic Model of CRLB

In this section, the CRLBs of the joint multiple parameter estimation are derived. The PDF of the complex echo signal y is given by

$$p(\mathbf{y}|\boldsymbol{\theta}) = \left(\frac{1}{\pi\sigma^2} \right)^N \exp\left\{ -\sum_{n=1}^{N} \frac{|y(n) - x(n)|^2}{\sigma^2} \right\}$$
$$= \prod_{n=1}^{N} \frac{1}{\pi\sigma^2} \exp\left\{ -\frac{|y(n) - x(n)|^2}{\sigma^2} \right\} \tag{15}$$

where $\boldsymbol{\theta}$ is the parameter vector to be estimated. The variables in the definition $\boldsymbol{\theta} = [\sigma^2|R|V|A_r|A_i]$ represent the variance of unknown noise, range, velocity, and real and imaginary parts of the amplitude, correspondingly. According to [1,2], the CRLB matrix for an unbiased estimate $\hat{\boldsymbol{\theta}}$ is the same as that in (7) and (8). We have

$$\nabla_\theta \ln p(\mathbf{x}|\theta) = \left[\frac{\partial}{\partial\sigma^2}, \frac{\partial}{\partial R}, \frac{\partial}{\partial V}, \frac{\partial}{\partial A_r}, \frac{\partial}{\partial A_i} \right]^T \tag{16}$$

Therefore, each item in the FIM can be calculated by

$$\mathbf{J}_{ij} = E\left[\frac{\partial \ln p(\mathbf{y}|\boldsymbol{\theta})}{\partial\theta_i} \frac{\partial \ln p(\mathbf{y}|\theta)^H}{\partial\theta_j} \right] \tag{17}$$

4.2. Series Expressions of Partial Derivative

The log-likelihood function can be obtained by taking the natural logarithm of (15)

$$\ln p(\mathbf{y}|\boldsymbol{\theta}) = \ln(\pi)^{-N} + \ln(\sigma^2)^{-N} + \left\{ -\frac{1}{\sigma^2} \sum_{n=1}^{N} |y(n) - x(n)|^2 \right\}$$
$$= -N\ln\pi - N\ln\sigma^2 - \frac{1}{\sigma^2} \left[(\mathbf{y} - \mathbf{x})^H (\mathbf{y} - \mathbf{x}) \right] \tag{18}$$

The partial derivative for the noise variance is derived:

$$\frac{\partial \ln p(\mathbf{y}|\boldsymbol{\theta})}{\partial\sigma^2} = -\frac{N}{\sigma^2} + \frac{1}{\sigma^4} \left[(\mathbf{y} - \mathbf{x})^H (\mathbf{y} - \mathbf{x}) \right] \tag{19}$$

Subsequently, the derivation for range is calculated as follows:

$$\frac{\partial \ln p(\mathbf{y}|\boldsymbol{\theta})}{\partial R} = -\frac{1}{\sigma^2} \frac{\partial \left[(\mathbf{y} - \mathbf{x})^H (\mathbf{y} - \mathbf{x}) \right]}{\partial R} \tag{20}$$

According to $\dfrac{\partial \mathbf{x}}{\partial R} = \dfrac{-j4\pi}{c}\mathbf{Fx}$, the partial derivation equation above can be written as

$$\frac{\partial \ln p(\mathbf{y}|\boldsymbol{\theta})}{\partial R} = -\frac{8\pi}{\sigma^2 c} \mathrm{Re}\left[(j\mathbf{Fx})^H \mathbf{w} \right] \tag{21}$$

Similarly, the partial derivative for the velocity term is $\dfrac{\partial \mathbf{x}}{\partial V} = \dfrac{-j4\pi T}{c}\mathbf{nFx}$.

$$\frac{\partial \ln p(\mathbf{y}|\boldsymbol{\theta})}{\partial V} = -\frac{8\pi T}{\sigma^2 c} \mathrm{Re}\left[(j\mathbf{nFx})^H \mathbf{w} \right] \tag{22}$$

For the real and imaginary parts of the amplitude, let $A = A_r + A_i$, the corresponding derivations are found respectively as follows

$$\frac{\partial \ln p(\mathbf{y}|\boldsymbol{\theta})}{\partial A_r} = -\frac{2}{\sigma^2}\text{Re}\left[\frac{1}{A^H}\mathbf{x}^H\mathbf{w}\right] \tag{23}$$

$$\frac{\partial \ln p(\mathbf{y}|\boldsymbol{\theta})}{\partial A_i} = \frac{2}{\sigma^2}\text{Re}\left[\frac{1}{A^H}(j\mathbf{x})^H\mathbf{w}\right] \tag{24}$$

From the deduction of the above, the integrated matrix can be expressed as

$$\nabla_\theta \ln p(\mathbf{x}|\theta) = \begin{bmatrix} -\dfrac{N}{\sigma^2}+\dfrac{1}{\sigma^4}\left[\mathbf{w}^H\mathbf{w}\right] \\[2mm] -\dfrac{8\pi}{\sigma^2 c}\text{Re}\left[(j\mathbf{Fx})^H\mathbf{w}\right] \\[2mm] -\dfrac{8\pi T}{\sigma^2 c}\text{Re}\left[(j\mathbf{nFx})^H\mathbf{w}\right] \\[2mm] -\dfrac{2}{\sigma^2}\text{Re}\left[\dfrac{1}{A^H}\mathbf{x}^H\mathbf{w}\right] \\[2mm] \dfrac{2}{\sigma^2}\text{Re}\left[\dfrac{1}{A^H}(j\mathbf{x})^H\mathbf{w}\right] \end{bmatrix} \tag{25}$$

4.3. Derivations of the FIM

The FIM elements are calculated in this section. (17) is split into the combinatorial form

$$\mathbf{J}_{\sigma^2 RV A_r A_i} = \begin{bmatrix} \mathbf{J}_{\sigma^2} & \mathbf{0} \\[2mm] \mathbf{0} & \begin{matrix} \mathbf{J}_{RV} & \mathbf{J}_{\overline{RV A_r A_i}} \\ \mathbf{J}_{\overline{A_r A_i RV}} & \mathbf{J}_{A_r A_i} \end{matrix} \end{bmatrix} \tag{26}$$

Because the measurement noise $\mathbf{w}$ obeys the complex normal distribution, some important properties are satisfied, as follows

$$\begin{aligned}
E\{\mathbf{w}\} &= \mathbf{0}_{N\times 1} \\
E\{\mathbf{w}\mathbf{w}^T\} &= \mathbf{0}_{N\times N} \\
E\{\mathbf{w}\mathbf{w}^H\} &= \sigma^2\mathbf{I}_{N\times N} \\
E\{\mathbf{w}^H\mathbf{w}\} &= N\sigma^2 \\
E\{\mathbf{w}^H\mathbf{w}\mathbf{w}^H\mathbf{w}\} &= N(N+1)\sigma^4 \\
E\{\mathbf{w}^*\mathbf{w}^T\} &= E\{(\mathbf{w}\mathbf{w}^H)^T\} = \sigma^2 \\
E\{\mathbf{w}^*\mathbf{w}^H\} &= E\{(\mathbf{w}\mathbf{w}^T)^*\} = \mathbf{0}_{N\times N}
\end{aligned} \tag{27}$$

Considering the variance of noise as a constant related to the distribution, the first item in (26) can be extracted for calculation. According to these properties, $\mathbf{J}_{\sigma^2}$ can be calculated by

$$\begin{aligned}
\mathbf{J}_{\sigma^2} &= \sigma^{-4}E\left[\frac{\partial \ln p(\mathbf{y}|\theta)}{\partial(\sigma^2)}\frac{\partial \ln p(\mathbf{y}|\theta)}{\partial(\sigma^2)}^H\right] \\
&= \sigma^{-4}E\left[N^2 - 2N\sigma^{-2}\mathbf{w}^H\mathbf{w} + \sigma^{-4}\mathbf{w}^H\mathbf{w}\mathbf{w}^H\mathbf{w}\right] \\
&= \sigma^{-4}N
\end{aligned} \tag{28}$$

A useful formula can be extracted to reduce the computational complexity. For two arbitrary matrices **P** and **Q**, the expectation after multiplying the real part of two matrices satisfies the following rule

$$
\begin{aligned}
&E\left[\operatorname{Re}\left(\mathbf{Pw}\right)\operatorname{Re}(\mathbf{Qw})^{H}\right]\\
&=\frac{1}{4}E\left[\left(\mathbf{Pw}+\mathbf{P}^{*}\mathbf{w}^{*}\right)\left(\mathbf{w}^{H}\mathbf{Q}^{H}+\mathbf{w}^{T}\mathbf{Q}^{T}\right)\right]\\
&=\frac{\sigma^{2}}{2}\operatorname{Re}(\mathbf{PQ}^{H})
\end{aligned}
\tag{29}
$$

Additionally, $\mathbf{\Gamma}=j\mathbf{Fx}$ is set to simplify the expression. It is apparent that $(j\mathbf{nFx})^{H}=\mathbf{\Gamma}^{H}\mathbf{n}$, where **n** is a real number diagonal matrix with $\mathbf{n}=\mathbf{n}^{H}=\mathbf{n}^{T}$. Substituting this symbol into $\mathbf{J}_{RV}$ and $\mathbf{J}_{A_{r}A_{i}}$ and calculating the expectation of the unbiased estimation error, every item in (26) can be simplified using this rule, which are

$$
\begin{aligned}
&E\left[\operatorname{Re}\left[\mathbf{\Gamma}^{H}\mathbf{w}\right]\operatorname{Re}\left[\mathbf{\Gamma}^{H}\mathbf{w}\right]^{H}\right]=\frac{1}{2}\sigma^{2}\operatorname{Re}(\mathbf{\Gamma}^{H}\mathbf{\Gamma})\\
&E\left[\operatorname{Re}\left[\mathbf{\Gamma}^{H}\mathbf{w}\right]\operatorname{Re}\left[\mathbf{\Gamma}^{H}\mathbf{nw}\right]^{H}\right]=\frac{1}{2}\sigma^{2}\operatorname{Re}(\mathbf{\Gamma}^{H}\mathbf{n\Gamma})\\
&E\left[\operatorname{Re}\left[\mathbf{\Gamma}^{H}\mathbf{nw}\right]\operatorname{Re}\left[\mathbf{\Gamma}^{H}\mathbf{w}\right]^{H}\right]=\frac{1}{2}\sigma^{2}\operatorname{Re}(\mathbf{\Gamma}^{H}\mathbf{n\Gamma})\\
&E\left[\operatorname{Re}\left[\mathbf{\Gamma}^{H}\mathbf{nw}\right]\operatorname{Re}\left[\mathbf{\Gamma}^{H}\mathbf{nw}\right]^{H}\right]=\frac{1}{2}\sigma^{2}\operatorname{Re}\left(\mathbf{\Gamma}^{H}\mathbf{n}^{2}\mathbf{\Gamma}\right)\\
&E\left[\operatorname{Re}\left(\frac{1}{A^{H}}\mathbf{x}^{H}\mathbf{w}\right)\operatorname{Re}\left(\mathbf{w}^{H}\mathbf{x}\frac{1}{A}\right)\right]=\frac{\sigma^{2}}{2}\operatorname{Re}\left(\frac{1}{AA^{H}}\mathbf{x}^{H}\mathbf{x}\right)\\
&E\left[-\operatorname{Re}\left(\frac{1}{A^{H}}\mathbf{x}^{H}\mathbf{w}\right)\operatorname{Re}\left(\mathbf{w}^{H}\left(j\mathbf{x}\right)\frac{1}{A}\right)\right]=\frac{\sigma^{2}}{2}\operatorname{Im}\left(\frac{1}{AA^{H}}\mathbf{x}^{H}\mathbf{x}\right)\\
&E\left[-\operatorname{Re}\left(\frac{1}{A^{H}}\left(j\mathbf{x}\right)^{H}\mathbf{w}\right)\operatorname{Re}\left(\mathbf{w}^{H}\mathbf{x}\frac{1}{A}\right)\right]=\frac{-\sigma^{2}}{2}\operatorname{Im}\left(\frac{1}{AA^{H}}\mathbf{x}^{H}\mathbf{x}\right)\\
&E\left[\operatorname{Re}\left(\frac{1}{A^{H}}\left(j\mathbf{x}\right)^{H}\mathbf{w}\right)\operatorname{Re}\left(\mathbf{w}^{H}\left(j\mathbf{x}\right)\frac{1}{A}\right)\right]=\frac{\sigma^{2}}{2}\operatorname{Re}\left(\frac{1}{AA^{H}}\mathbf{x}^{H}\mathbf{x}\right)
\end{aligned}
\tag{30}
$$

To integrate the processes above, the submatrices can be written as follows.

$$
\mathbf{J}_{RV}=\frac{32\pi^{2}}{\sigma^{2}c^{2}}\left[\begin{array}{cc}\operatorname{Re}(\mathbf{\Gamma}^{H}\mathbf{\Gamma}) & T\operatorname{Re}(\mathbf{\Gamma}^{H}\mathbf{n\Gamma})\\ T\operatorname{Re}(\mathbf{\Gamma}^{H}\mathbf{n\Gamma}) & T^{2}\operatorname{Re}\left(\mathbf{\Gamma}^{H}\mathbf{n}^{2}\mathbf{\Gamma}\right)\end{array}\right]
\tag{31}
$$

$$
\mathbf{J}_{A_{r}A_{i}}=\frac{\sigma^{2}}{2}\left[\begin{array}{cc}\operatorname{Re}\left(\frac{1}{AA^{H}}\mathbf{x}^{H}\mathbf{x}\right) & \operatorname{Im}\left(\frac{1}{AA^{H}}\mathbf{x}^{H}\mathbf{x}\right)\\ -\operatorname{Im}\left(\frac{1}{AA^{H}}\mathbf{x}^{H}\mathbf{x}\right) & \operatorname{Re}\left(\frac{1}{AA^{H}}\mathbf{x}^{H}\mathbf{x}\right)\end{array}\right]
\tag{32}
$$

The remaining eight items in **J** can be obtained separately, which are

$$
\begin{aligned}
E(R,A_{r})&=E\left[\frac{\partial\ln p(\mathbf{y}|\theta)}{\partial(R)}\frac{\partial\ln p(\mathbf{y}|\theta)}{\partial(A_{r})}^{H}\right]\\
&=E\left[\left(-\frac{8\pi}{\sigma^{2}c}\operatorname{Re}\left[\mathbf{\Gamma}^{H}\mathbf{w}\right]\right)\left(-\frac{2}{\sigma^{2}}\right)\operatorname{Re}\left[\frac{1}{A^{H}}\mathbf{x}^{H}\mathbf{w}\right]^{H}\right]\\
&=\frac{16\pi}{\sigma^{4}c}\frac{\sigma^{2}}{2}\operatorname{Re}\left(\frac{1}{A}\mathbf{\Gamma}^{H}\mathbf{x}\right)=\frac{8\pi}{\sigma^{2}c}\operatorname{Im}(\frac{1}{A}\mathbf{x}^{H}\mathbf{F}^{H}\mathbf{x})
\end{aligned}
\tag{33}
$$

The similar results are given by

$$E(R, A_i) = E\left[\frac{\partial \ln p(\mathbf{y}|\theta)}{\partial(R)} \frac{\partial \ln p(\mathbf{y}|\theta)}{\partial(A_i)}^H\right] = -\frac{8\pi}{\sigma^2 c}\mathrm{Re}(\frac{1}{A}\mathbf{x}^H\mathbf{F}^H\mathbf{x})$$

$$E(V, A_r) = E\left[\frac{\partial \ln p(\mathbf{y}|\theta)}{\partial(V)} \frac{\partial \ln p(\mathbf{y}|\theta)}{\partial(A_i)}^H\right] = \frac{8\pi T}{\sigma^2 c}\mathrm{Im}\left(\frac{1}{A}\mathbf{x}^H\mathbf{F}^H\mathbf{n}^H\mathbf{x}\right)$$

$$E(V, A_i) = E\left[\frac{\partial \ln p(\mathbf{y}|\theta)}{\partial(V)} \frac{\partial \ln p(\mathbf{y}|\theta)}{\partial(A_i)}^H\right] = -\frac{8\pi T}{\sigma^2 c}\mathrm{Re}\left(\frac{1}{A}\mathbf{x}^H\mathbf{F}^H\mathbf{n}^H\mathbf{x}\right)$$

$$E(A_r, R) = E\left[\frac{\partial \ln p(\mathbf{y}|\theta)}{\partial(A_r)} \frac{\partial \ln p(\mathbf{y}|\theta)}{\partial(R)}^H\right] = -\frac{8\pi}{\sigma^2 c}\mathrm{Im}\left(\frac{1}{A^H}\mathbf{x}^H\mathbf{F}\mathbf{x}\right) \qquad (34)$$

$$E(A_r, V) = E\left[\frac{\partial \ln p(\mathbf{y}|\theta)}{\partial(A_r)} \frac{\partial \ln p(\mathbf{y}|\theta)}{\partial(V)}^H\right] = -\frac{8\pi T}{\sigma^2 c}\mathrm{Im}\left(\frac{1}{A^H}\mathbf{x}^H\mathbf{n}\mathbf{F}\mathbf{x}\right)$$

$$E(A_i, R) = E\left[\frac{\partial \ln p(\mathbf{y}|\theta)}{\partial(A_i)} \frac{\partial \ln p(\mathbf{y}|\theta)}{\partial(R)}^H\right] = -\frac{8\pi}{\sigma^2 c}\mathrm{Re}\left(\frac{1}{A^H}\mathbf{x}^H\mathbf{F}\mathbf{x}\right)$$

$$E(A_i, V) = E\left[\frac{\partial \ln p(\mathbf{y}|\theta)}{\partial(A_i)} \frac{\partial \ln p(\mathbf{y}|\theta)}{\partial(R)}^H\right] = -\frac{8\pi T}{\sigma^2 c}\mathrm{Re}\left(\frac{1}{A^H}\mathbf{x}^H\mathbf{n}\mathbf{F}\mathbf{x}\right)$$

Another two submatrices are summarized as

$$\mathbf{J}_{\overline{RVA_rA_i}} = \frac{8\pi}{\sigma^2 c}\begin{bmatrix} \mathrm{Im}(\frac{1}{A}\mathbf{x}^H\mathbf{F}^H\mathbf{x}) & -\mathrm{Re}(\frac{1}{A}\mathbf{x}^H\mathbf{F}^H\mathbf{x}) \\ T\mathrm{Im}\left(\frac{1}{A}\mathbf{x}^H\mathbf{F}^H\mathbf{n}^H\mathbf{x}\right) & -T\mathrm{Re}\left(\frac{1}{A}\mathbf{x}^H\mathbf{F}^H\mathbf{n}^H\mathbf{x}\right) \end{bmatrix} \qquad (35)$$

$$\mathbf{J}_{\overline{A_rA_iRV}} = -\frac{8\pi}{\sigma^2 c}\begin{bmatrix} \mathrm{Im}\left(\frac{1}{A^H}\mathbf{x}^H\mathbf{F}\mathbf{x}\right) & T\mathrm{Im}\left(\frac{1}{A^H}\mathbf{x}^H\mathbf{n}\mathbf{F}\mathbf{x}\right) \\ \mathrm{Re}\left(\frac{1}{A^H}\mathbf{x}^H\mathbf{F}\mathbf{x}\right) & T\mathrm{Re}\left(\frac{1}{A^H}\mathbf{x}^H\mathbf{n}\mathbf{F}\mathbf{x}\right) \end{bmatrix} \qquad (36)$$

Based upon the previous derivation, the complete FIM is presented in (37) by substituting the results of the submatrices into the original (26). Subsequently, the values of the CRLBs, which characterize the estimated performance, can be calculated by substituting this FIM into (7).

$$\mathbf{J} = \begin{bmatrix} \sigma^{-4}N & \mathbf{0} & & \mathbf{0} \\ & \frac{32\pi^2}{\sigma^2\varsigma^2}\mathrm{Re}(\mathbf{x}^H\mathbf{F}^H\mathbf{F}\mathbf{x}) & \frac{32\pi^2}{\sigma^2\varsigma^2}T\mathrm{Re}(\mathbf{x}^H\mathbf{F}^H\mathbf{n}\mathbf{F}\mathbf{x}) & \frac{8\pi}{\sigma^2 c}\mathrm{Im}\left(\frac{1}{A}\mathbf{x}^H\mathbf{F}^H\mathbf{x}\right) & -\frac{8\pi}{\sigma^2 c}\mathrm{Re}(\frac{1}{A}\mathbf{x}^H\mathbf{F}^H\mathbf{x}) \\ \mathbf{0} & \frac{32\pi^2}{\sigma^2 c^2}T\mathrm{Re}(\mathbf{x}^H\mathbf{F}^H\mathbf{n}\mathbf{F}\mathbf{x}) & \frac{32\pi^2}{\sigma^2 c^2}T^2\mathrm{Re}(\mathbf{x}^H\mathbf{F}^H\mathbf{n}^2\mathbf{F}\mathbf{x}) & \frac{8\pi T}{\sigma^2 c}\mathrm{Im}\left(\frac{1}{A}\mathbf{x}^H\mathbf{F}^H\mathbf{n}^H\mathbf{x}\right) & -\frac{8\pi T}{\sigma^2 c}\mathrm{Re}\left(\frac{1}{A}\mathbf{x}^H\mathbf{F}^H\mathbf{n}^H\mathbf{x}\right) \\ & -\frac{8\pi}{\sigma^2 c}\mathrm{Im}\left(\frac{1}{A^H}\mathbf{x}^H\mathbf{F}\mathbf{x}\right) & -\frac{8\pi T}{\sigma^2 c}\mathrm{Im}\left(\frac{1}{A^H}\mathbf{x}^H\mathbf{n}\mathbf{F}\mathbf{x}\right) & \frac{\sigma^2}{2}\mathrm{Re}\left(\frac{1}{AA^H}\mathbf{x}^H\mathbf{x}\right) & \frac{\sigma^2}{2}\mathrm{Im}\left(\frac{1}{AA^H}\mathbf{x}^H\mathbf{x}\right) \\ \mathbf{0} & -\frac{8\pi}{\sigma^2 c}\mathrm{Re}\left(\frac{1}{A^H}\mathbf{x}^H\mathbf{F}\mathbf{x}\right) & -\frac{8\pi T}{\sigma^2 c}\mathrm{Re}\left(\frac{1}{A^H}\mathbf{x}^H\mathbf{n}\mathbf{F}\mathbf{x}\right) & -\frac{\sigma^2}{2}\mathrm{Im}\left(\frac{1}{AA^H}\mathbf{x}^H\mathbf{x}\right) & \frac{\sigma^2}{2}\mathrm{Re}\left(\frac{1}{AA^H}\mathbf{x}^H\mathbf{x}\right) \end{bmatrix} \qquad (37)$$

5. CRLB of Sparse Based Estimator—Compressive Sensing

Compressive sensing is applicable to the sparse target recovery model for this type of undersampled signal. Unlike the performance analysis above, this method presents its own evaluation criteria when calculating the estimation performance. In this section, the CRLB performance for a CS with an SSF signal is analyzed.

In the receiving signal (3), the spaces of the range and velocity can be divided into $P \times Q$ grids. The dimensions of the range are $[R_1, R_2, \cdots, R_P]$. Similarly, the dimensions of the velocity are $[V_1, V_2, \cdots, V_Q]$. Therefore, the range unit can be written as $\Delta R = c/(2\Delta f P)$, and the velocity unit can be written as $\Delta V = c/(2f_0 T Q)$. At every grid, the target exhibits the corresponding scattering intensity, that is

$$x(p,q) = \begin{cases} A, \text{The } ((p-1)Q+q)^{th} \text{grid exists a target} \\ 0, \text{The target is not located at } ((p-1)Q+q)^{th} \text{ grid} \end{cases} \tag{38}$$

The phase of the echo signal is redefined as

$$\Phi_i\left(m, (p-1)Q+q\right) = \exp(j4\pi(f_0 + m\Delta f)(R_p + V_q mT)/c), \tag{39}$$

where $m \in [1, 2, ..., M], p \in [1, 2, ..., P], q \in [1, 2, ..., Q]$, and every Φ_i is an $M \times 1$ column vector representing the phase shift on M pulses caused by the target at the position of the ith grid. Therefore, Φ is the combination of all possible phase shifts on range velocity grids. Researchers in [24,25] have deduced the CRLB for estimating the sparse parameter. Additionally, we can obtain the performance representation from the FIM. Similar to the same concept of (7) and (8), we have

$$\mathbf{J}_{ij} = \frac{1}{\sigma^2}\left(\Phi_I^H \Phi_I\right)_{ij} \tag{40}$$

where I is the index set defined in the columns of submatrix Φ_I from Φ. Therefore, the unbiased estimation by the CRLB is

$$E\left\{\|\hat{\mathbf{x}} - \mathbf{x}\|^2\right\} \geq Tr(\mathbf{J}^{-1}) = \sigma^2 Tr\left(\left(\Phi_I^H \Phi_I\right)^{-1}\right) \tag{41}$$

The performance characterization is related to only Φ. This rule is appropriate for the sparse target estimation. However, it is noticeable that, after compressive sensing reconstruction, the recovered results are subsequently mapped inversely to the corresponding real range velocity unit as the subscript. The largest K values are transformed into $\hat{\mathbf{x}}$. If the subscript of the maximum value is located at one position $\hat{x}_k$ in all scopes PQ, the real range and velocity estimations are determined by calculation. Specifically, $R_k = \Delta R * \beta$, $V_k = \text{mod}(\hat{x}_k, \beta)$, where $\beta = \lfloor \hat{x}_k/Q \rfloor$, $\lfloor \cdot \rfloor$ is the rounding operator, $\text{mod}(a, b)$ denotes the remaining operators from a to b. The sparse targets can subsequently be reconstructed accurately.

6. Experiments and Discussion

This section introduces several simulations to examine how the CRLB performs when the parameters are changed. The discussions above are compared herein.

6.1. CRLB Comparison with Different Waveforms

According to the deviation of the time delay and Doppler stretch model, we generate the CRLB by various waveforms in different parameter configurations for comparison. These waveforms include LFM_1 and LFM_2 with changing pulse width and total bandwidth, LSF_1 and LSF_2 with changing pulse number and total bandwidth, two SSF waveforms with changing envelope, namely $\text{SSF}_{\text{chirp}}$ (13) and SSF_{rect} (14). In each trial, the value of SNR is set from 0 to 40 dB. Other basic parameters are $T_w = 1$ ms, $T = 2$ ms, $M = 100$, $N = 50$, $\Delta f = 50$ kHz, $f_0 = 10$ MHz. The theoretical CRLB for time delay and Doppler stretch estimation are respectively illustrated in Figure 1a,b. For the legends [A,B,C] in the figure, three parts represent the total number of pulses in a burst, pulse width for each pulse, and equivalent coverage bandwidth. "M in order" represents the using frequencies from 0 to $M-1$ multiples of Δf in sequence. "Random N from M" means N frequencies combination is generated as the rule of SSF from frequency span $M\Delta f$.
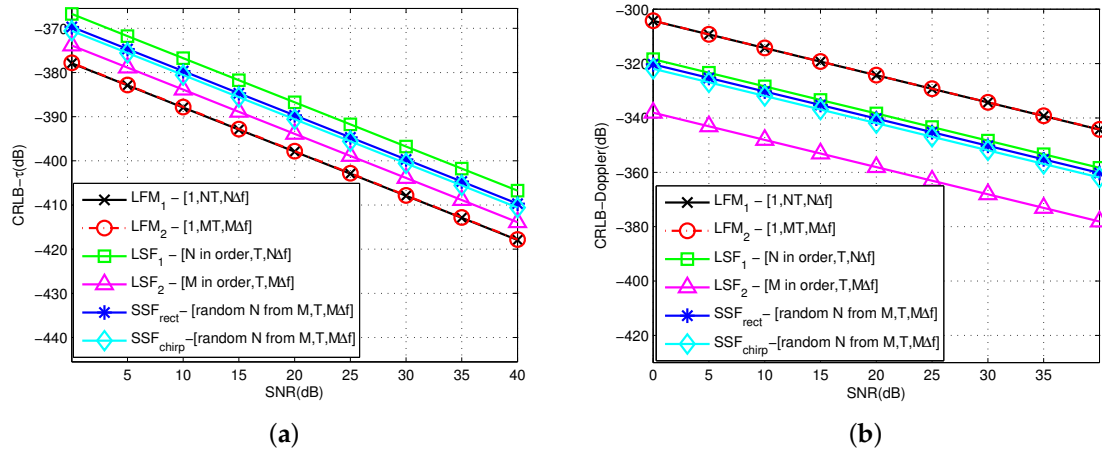
Figure 1. Comparison of CRLBs with different waveform. (**a**) CRLB of time delay; (**b**) CRLB of Doppler-stretch.

As shown in the figure, the performance trend of the estimation from multiple waveforms is consistent along with the increasing SNR under the same basic parameters. However, the difference exists between time estimation and Doppler estimation. For time delay estimation, the CRLB of SF-based waveforms are obviously not as good as that of LFM signal, but have better performance in Doppler estimation. When the bandwidth range and pulse width change, it has slight influence on the estimation for LFM. With the increasing bandwidth in LSF, the performance improves significantly. By comparison, the CRLB of SSF with N sparse frequencies is used between N pulses and M pulses in LSF signal. Moreover, the envelope plays an insignificant role.

6.2. Comparison of Different CRLBs

For the deviations in the time delay and Doppler stretch model, we use the CRLB of SSF-chirp signal as an example. The obtained statistical rules are also applied to the SSF-rect and LSF signals based on a reasonable definition of variables.

For each SNR value from 0 to 40 dB, we calculate the theoretical $\text{var}(\hat{\tau})_{ship}$ of 500 independent Monte Carlo simulations. In each trial, the frequency combination is generated randomly from the frequency span. The basic parameters are $T_w = 1$ ms, $T = 5$ ms, $M = 100$, $N = 50$, $\Delta f = 1$ KHz, $f_0 = 5$ MHz. The estimation performances with different frequency steps are illustrated in Figure 2a. The basic parameters are set as the above setting while Δf is set to 0 kHz, 50 kHz, 100 kHz, and 200 kHz for comparison. Similarly, f_0 is set to 5 MHz, 15 MHz, 25 MHz and 35 MHz in Figure 2b; frequency number N is set to 10, 40, 70, and 100 in Figure 2c. Any four groups of sparse frequency combination are selected from all the tests to compare in Figure 2d.

As shown in the figure, the changes in Δf, f_0, and N exhibit corresponding effects on the range of the final CRLB. However, only Δf exhibits uniform variations, the other two variables exhibit differentiations under equidistant values. The effect of random combination is minimal when the other conditions remain unchanged.

The CRLB of the joint multiple parameter estimation is the same as in (4). Every normalized CRLB_i as the ith independent parameter can also be calculated individually. For every SNR value from 0 to 50 dB, the theoretical CRLB is calculated. In each trial, the frequency combination is generated randomly within the frequency span. The other basic parameters are the same as that in the first simulation. The target information to be estimated is set as $R = 5$ km, $V = 2$ m/s, $A = 0.5 + 0.8j$.
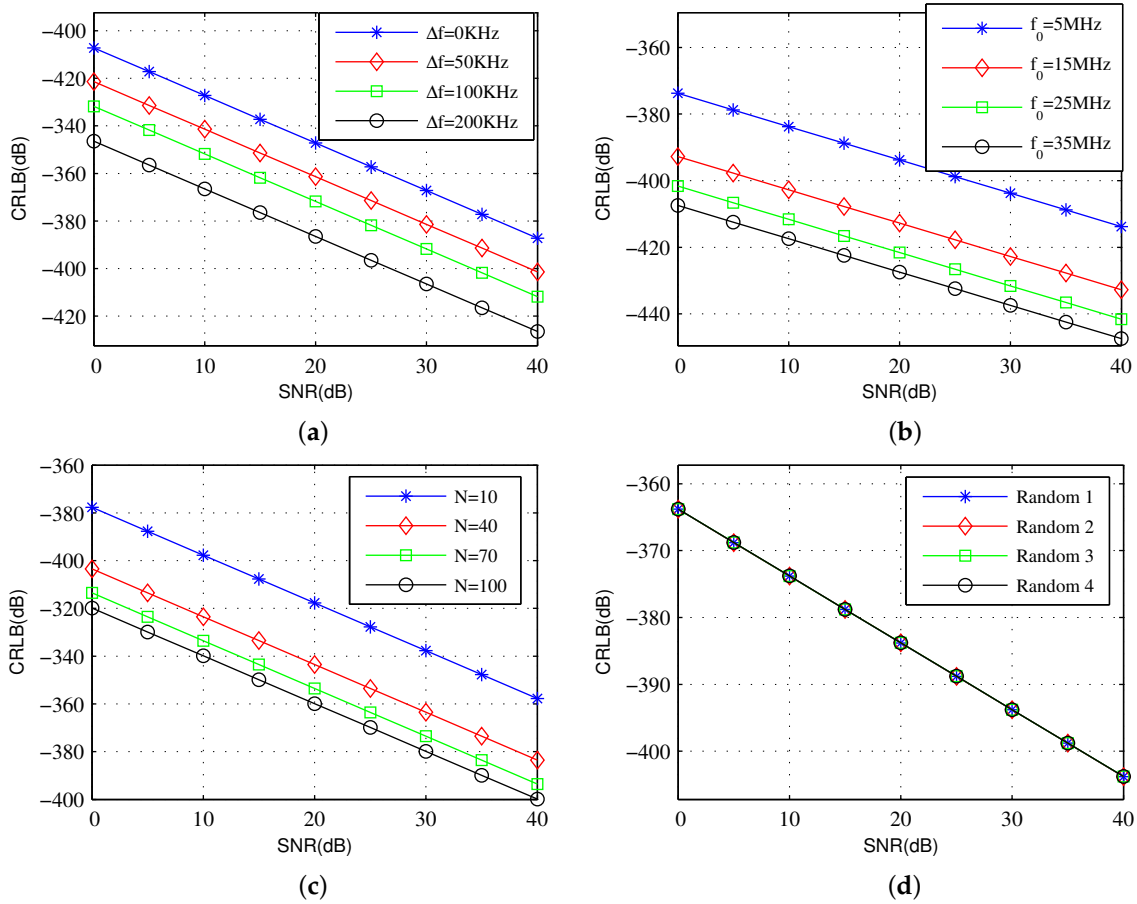
Figure 2. CRLB comparison with different parameters. (**a**) different frequency step ; (**b**) different initial carrier frequency; (**c**) different frequency number; (**d**) different sparse frequency combination.

The estimation performance of every CRLB$_i$ is illustrated in Figure 3a. It shows the contribution of each separated value to the overall CRLB by changing the SNR. If the best estimation performance is synthesized, the parameters related to the single coefficient to be estimated can be adjusted appropriately.

To observe the trend of performance caused by various parameters more intuitively, a statistical analysis is presented in Figure 2b. The differences of the effects from various factors on the estimation performance are shown clearly. For each group of parameters, 500 independent Monte Carlo simulations are performed to obtain a statistical trend. The primary parameters of the variables are shown in Table 1.

Table 1. Parameters setting for multiple groups of SSF signal.

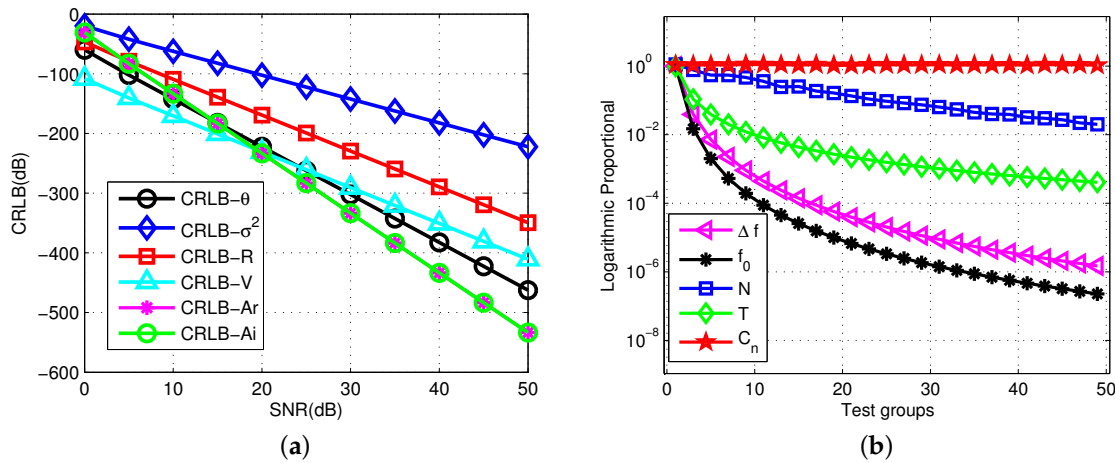| Variables	Initial Value	the Value of ith Groups	Value Range
σ^2	$(\sigma^2)^{(0)} = 1$	$(\sigma^2)^{(i)} = 10^{2(i/20)}$	$i = [1, 50]$
Δf (kHz)	$\Delta f^{(0)} = 1$	$\Delta f^{(i)} = \Delta f^{(0)} + (10i - 1)$	$i = [1, 50]$
f_0 (MHz)	$f_0^{(0)} = 1$	$f_0^{(i)} = f_0^{(0)} + (i - 1)$	$i = [1, 50]$
N	$N^{(0)} = 40$	$N^{(i)} = N^{(0)} + (i - 1)$	$i = [1, 50]$
T(ms)	$T^{(0)} = 1$	$T^{(i)} = T^{(0)} + (i - 1)$	$i = [1, 50]$
C	Random	Random	$C_n \in [1, M]$

Figure 3. Comparison of CRLBs with changing SNR. (**a**) Monte Carlo Comparison of CRLBs; (**b**) Monte Carlo simulation of CRLB-*θ* with multiple variables.

$(\cdot)^{(0)}$ represents the initial value for any variables; $(\cdot)^{(i)}$ represents the value in the ith group. When testing a variable, other variables are defined as the initial value. For the parameters of every group, the logarithmic proportional function is used to characterize the trend, that is $P(i) = \log \dfrac{\text{var}(\cdot)^{(i)}}{\text{var}(\cdot)^{(0)}}$. The testing variables are the frequency combination coefficient **C**, frequency number N, environment parameter σ^2, PRI T, frequency step Δf and initial carrier frequency f_0. As shown in the figure, the changes in Δf, f_0, and N exhibit corresponding effects on the range of the final CRLB. However, only Δf exhibits uniform variations; the other two variables exhibit differentiations under equidistant values. The effect of random combination is minimal when the other conditions remain unchanged.

The related parameters are divided broadly into the following categories.

Envelope of signal: When $\gamma = 0$, $\text{var}(\cdot)_{chirp} = \text{var}(\cdot)_{rect}$. The value of γ has little effect. Because the value is sufficiently small, and the most of this coefficient concentrate in the items of n sequence with $f_n >> n > \gamma$, it implies that the envelope is not the dominant factor.

SNR, velocity, and amplitude: The real coefficient containing π, c, and σ^2 will directly affect the calculation results. The three items N_0, σ, $|a|$ are related to the SNR, velocity, and amplitude, respectively. The SNR can be obtained from the power and PSD, namely, $SNR = E/N_0$. Specifically, CRLB is proportional to σ, and inversely proportional to N_0.

Sparse frequency combination, frequency number N: When the value of N is fixed, the using signal bandwidth and the synthetic bandwidth are constant for each sparse frequency combination. Thus, the combination of frequencies does not have a significant effect. However, the maximum interval between two frequencies and the dispersion of every combination will impose higher requirements on the recovery method. Different methods involve particular constraints on the relationship between N and M, as well as special requirements for the rule of frequency hopping. We will not discuss this in detail; only the performance comparison will be emphasized herein.

Initial carrier frequency, pulse width, frequency step, and PRI: These parameters are determined by the signal, and are not changed by the environment and target scene. The trends of the three parameters is are synchronized. The value of f_0 is typically large, reaching MHz or even GHz, which is significantly larger than any other parameters. Therefore, it is the most significant factor. Conversely, T and T_w are negligible owing to their small magnitudes.

6.3. CRLBs Using Different Estimators

This simulation uses the bound comparison produced by different estimators. The symbols C1, C2, and C3 are used to represent the time delay and Doppler stretch estimator, joint multiple parameter estimator, and sparse based estimator, respectively. The comparison results are shown in Figure 4.

The general parameters are set with $T_w = 1$ ms, $T = 4$ ms, $M = 50$, $N = 80$, $\Delta f = 1$ kHz, $R_0 = 15$ km, $V_0 = 2$ m/s, $A_0 = -0.5 + 0.5j$, and the SNR is changed from 0 to 30 dB. In Figure 4a, the sampling rule includes the uniform M frequencies in M pulses, uniform N frequencies in N pulses, and random M sequences from N frequencies with M pulses. The time delay τ and Doppler stretch σ estimation are tested. In Figure 4b, the primary target information is measured: target range R, velocity V, and amplitude A under different sampling models. Jointly, the obtained overall CRLB *C2-All* is shown in the same figure. In Figure 4c, the sparse estimation is considered with the method based on grid partition. Therefore, it depends on the numbers of range grids GR and velocity grids GV. We use three groups of different grid numbers as an example.
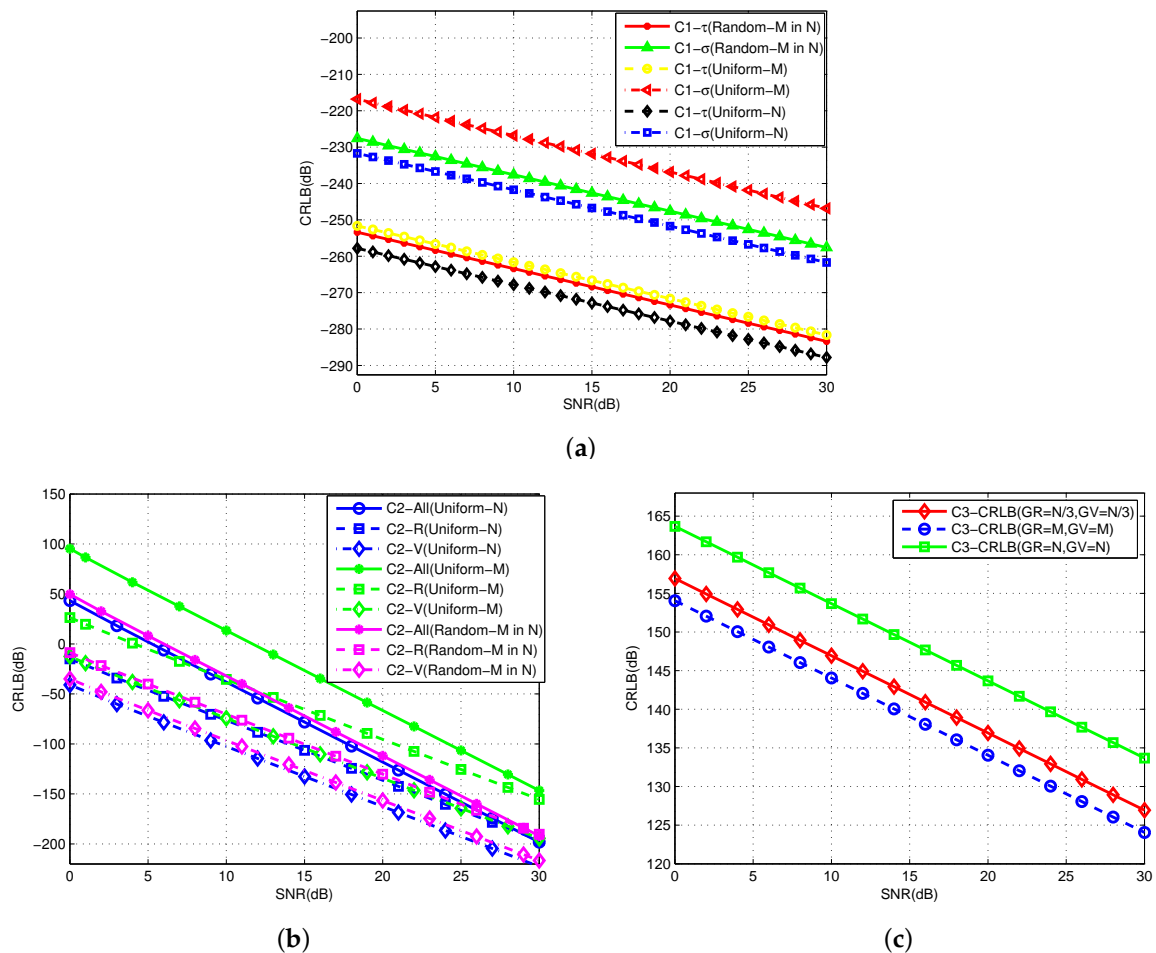

(a)

(b)

(c)

Figure 4. Comparison of CRLBs using different model. (**a**) CRLB using time delay and Doppler stretch estimator; (**b**) CRLB using multiple parameter estimator; (**c**) CRLB using the sparse based estimator.

As shown in the figure, the CRLB index is changed owing to the different samplings. In the uniform samplings, more samplings produce better estimation performance. However, the transmitting frequencies chosen randomly are somewhere in between. Therefore, we conclude from the statistical estimation, part of the estimation can be consistent with the theoretical value, while the estimation performance remains unchanged when the SNR is large.

6.4. RD Comparison between Different Methods

A practical example is presented to demonstrate the effectiveness of the target location using different estimation methods. We use the IDFT method, correlation function method [18], and CS method to estimate the range and velocity as a practical example. The contrasting figures illustrate the effect of resolution improvement and sidelobe suppression in the range domain. An SSF transmitting signal is designed using all available frequencies. The system parameters are set with carrier frequency $f_0 = 7.5$ MHz, sample frequency $f_s = 1$ kHz, pulse width $T_w = 1$ ms, PRI $T = 4$ ms, frequency span is 500 kHz, pulse number $M = 250$, step size $\Delta f = 1$ kHz. Six targets are considered with the parameter configuration as (#1) $R_1 = 258$ km, $V_1 = 3$ m/s, (#2) $R_2 = 258$ km, $V_2 = 6$ m/s, (#3) $R_3 = 251$ km, $V_3 = 0$ m/s, (#4) $R_4 = 250$ km, $V_4 = 0$ m/s, (#5) $R_5 = 244$ km, $V_5 = -1$ m/s, (#6) $R_6 = 240$ km, $V_6 = -5$ m/s. The SNR for every target is set to the same value 20 dB. Thus, the frequency utilization rate is only 46%. We set multiple moving targets in the line-of-sight with the range and velocity values shown in Figure 5d.

Targets #3 and #4 are located at a close proximity with the same (zero) velocity. For the convenience of observation, the targets are shown with the same amplitude and SNR. Two-dimensional signal processing for the echo signals is performed from 50 burst pulses transmitted continuously. Processing methods are used to estimate the information of the targets. The comparison results of the three methods are shown in Figure 5a–c.
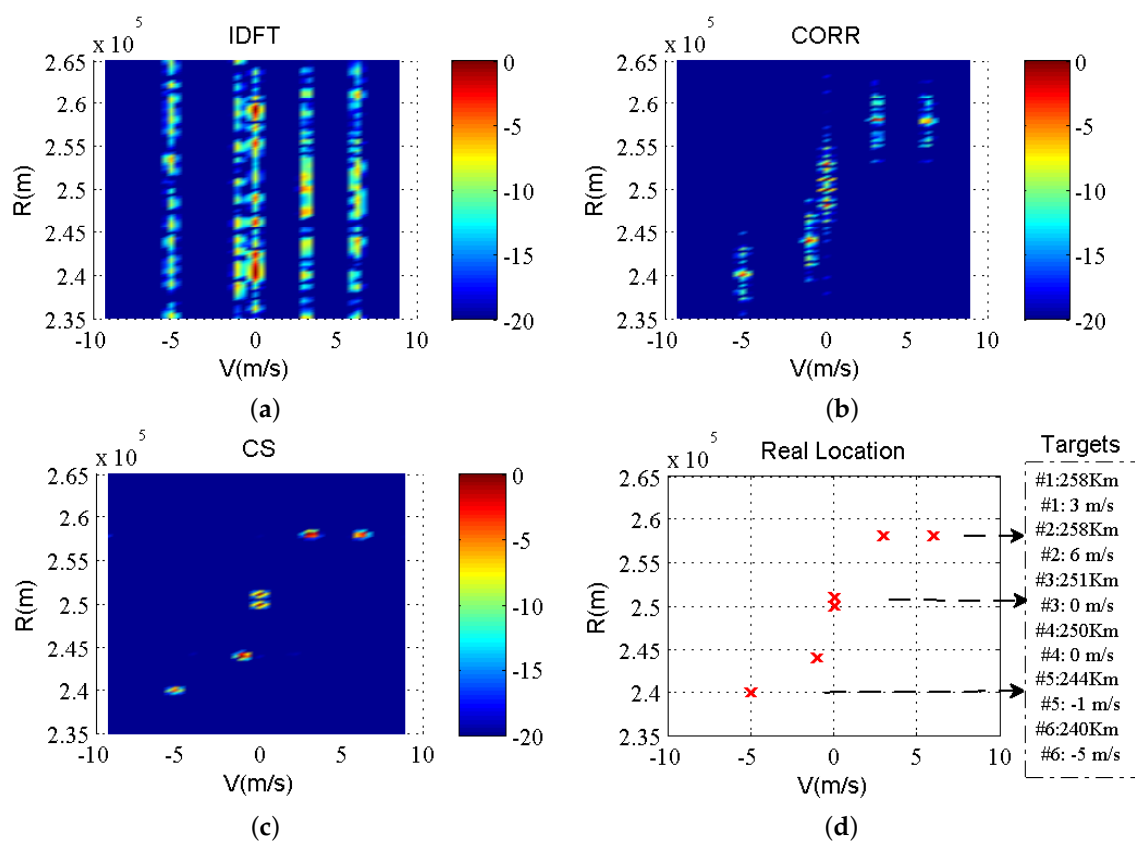

Figure 5. Target RD estimation with different method. (**a**) IDFT method; (**b**) Correlation function method; (**c**) compressive sensing method; (**d**) actual location of targets as a reference (The theoretical values of the actual range and velocity location are the discrete points in (**d**), which only provide references for estimation in (**a**) (**b**) and (**c**)).

It is apparent that the IDFT method cannot determine the location of the targets. The range and velocity information of the targets can be obtained by the correlation function method. However, owing to the effect of the high-range sidelobe level, this method cannot distinguish the exact location

of the targets. If we do not consider the ambiguity caused by the radial velocity, and only focus on the sidelobe suppression in the range domain, the CS method yields a better performance in improving the precision of the range measurement. The selected observation range of the axis is −20 to 0 dB. As shown, the sidelobe below −20 dB have little effect on the targets; additionally, it is easy to distinguish two closely spaced targets.

Next we will give a statistical result for IDFT, CORR and CS method. In Figure 6, by adding the range, velocity and the amplitude estimated error together, the statistical values of the minimum mean square error (MMSE) are tested by Monte Carlo simulations. The times of Monte Carlo is 500, SNR from 0 to 30 dB. For CS, the traditional orthogonal matching pursuit method is chosen here. Three different methods are drawn separately because of the difference in error value level. Figure 6a illustrates the MMSE of IDFT and CORR method. The results of comparison between CRLB and MMSE of CS method are shown in Figure 6b.
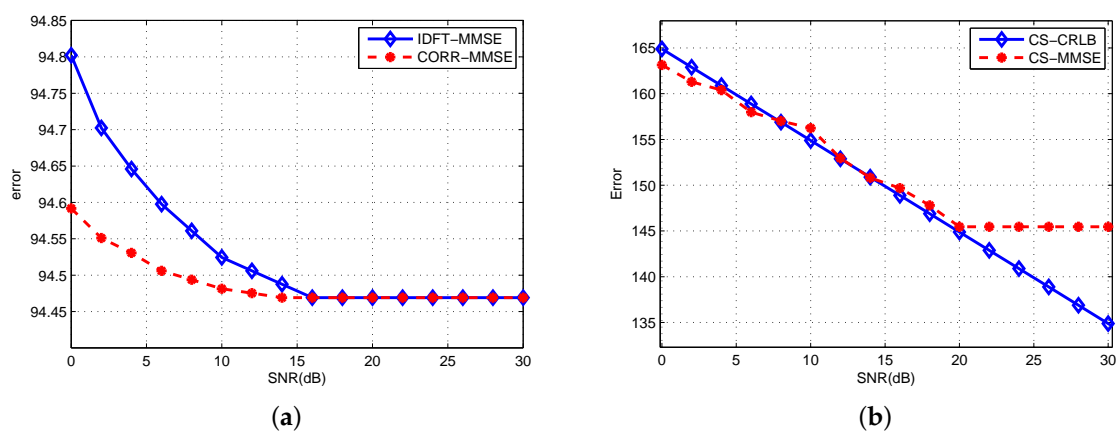

Figure 6. Monte Carlo tests of target estimation. (**a**) MMSE of IDFT and CORR method; (**b**) CRLB and MMSE of CS method.

As shown in the figure, with the increase of SNR, the trend of MMSE is decreased before stable in a certain value until it reaches a large SNR. CORR method has the fastest speed to achieve stable accuracy, and CS method has the best robustness in this test. The results of theoretical CRLB and MMSE are consistent with CS method. When SNR exceeds 20 dB, the limitation of grids will lead to a same error without further reduction.

7. Conclusions

In this paper, the CRLB performance by different representations was analyzed under the conversion of multiple equivalent models. Several theoretical derivations were investigated for different estimation methods; they will serve as reference and guidance for the design of transmission waveforms in the front end and the estimation of signals in the back end. With these specific expressions, the estimation performances for different parameter combinations could be determined directly. With increasing Δf, f_0, N, and T, CRLB performance was improved. Additionally, environmental noise as an extremely important factor should be considered. Meanwhile, regarding the determined frequency width, the effect of frequency combination based on statistics was much weaker for this type of signal. The theoretical results are beneficial for target estimation and detection by introducing an SSF signal into a radar system.

Author Contributions: conceptualization, Q.C., X.Z. and Q.Y.; writing—original draft preparation, Q.C.; methodology, Q.C., M.Z.; formal analysis, M.Z.; investigation, L.Y.; writing—review and editing, Q.C. and Q.Y.; visualization, L.Y. and X.Z.; supervision, L.Y. and Q.Y.; funding acquisition, Q.Y. and X.Z.

Conflicts of Interest: The authors declare no conflict of interest.

References

1. Scharf, L.; Mcwhorter, L. Geometry of the Cramér-Rao bound. In Proceedings of the IEEE 6th SP Workshop on Statistic Signal and Array Process, Victoria, BC, Canada, 7–9 October 1992; pp. 5–8.
2. Jin, Q.; Wong, K.; Luo, Z. The estimation of time delay and Doppler stretch of wideband signals. *IEEE Trans. Signal Process.* **1995**, *43*, 904–916. [CrossRef]
3. Shi, C.; Salous, S.; Wang, F.; Zhou, J. Cramér-Rao Lower Bound Evaluation for Linear Frequency Modulation Based Active Radar Networks Operating in a Rice Fading Environment. *Sensors* **2016**, *16*, 2072. [CrossRef] [PubMed]
4. Shi, C.; Wang, F.; Salous, S.; Zhou, J. Cramér-Rao lower bounds for joint target parameter estimation in FM-based distributed passive radar network with antenna arrays. *Radio Sci.* **2018**, *53*, 314–333. [CrossRef]
5. Shi, C.; Wang, F.; Zhou, J. Cramér-rao bound analysis for joint target location and velocity estimation in frequency modulation based passive radar networks. *IET Signal Process.* **2016**, *10*, 780–790. [CrossRef]
6. Shi, C.; Wang, F.; Salous, S. Performance Analysis for Joint Target Parameter Estimation in UMTS-Based Passive Multistatic Radar with Antenna Arrays Using Modified Cramer-Rao Lower Bounds. *Sensors* **2017**, *17*, 2379. [CrossRef] [PubMed]
7. Tilli, E.; Ortenzi, L.; Prodi, F. On the use of HRR data to improve target kinematics estimation: CRLB computation and comparison with simulated results. In Proceedings of the IEEE Radar Conference, Washington, DC, USA, 10–14 May 2010; pp. 380–384.
8. Xiong, J.; Ouyang, X.; Luo, L. A novel Cramér-rao lower bound of time difference of arrival for frequence hopping signals. In Proceedings of the 5th International Congress on Image and Signal Processing, Chongqing, China, 16–18 October 2012; pp. 1741–1744.
9. Zhang, N.; Zhao, T.; Huang, T. Cramér-rao lower bounds of joint time delay and Doppler-stretch estimation with random stepped-frequency signals. In Proceedings of the IEEE International Conference on Digital Signal Processing (DSP), Beijing, China, 16–18 October 2016; pp. 647–651.
10. Zhao, T.; Zhang N.; Huang, T. Performance analysis of joint time delay and Doppler-stretch estimation with random stepped-frequency signals. In Proceedings of the IEEE International Conference on Digital Signal Processing, Beijing, China, 16–18 October 2016; pp. 594–598.
11. Zhou, J.; Zhao, H; Shi, Z. Analytic performance bounds on estimates of scattering center parameters. *Trans. Aerosp. Electron. Syst.* **2007**, *43*, 813–826. [CrossRef]
12. Zhou, J.; Zhao, H.; Shi, Z. Performance Analysis of 1D Scattering Center Extraction From Wideband Radar Measurements. In Proceedings of the IEEE International Conference on Acoustics, Speech and Signal Processing (ICASSP 2006), Toulouse, France, 14–19 May 2006.
13. Wei, H.; Ye, S.; Wan, Q. Influence of phase on Cramer-Rao lower bounds for joint time delay and Doppler stretch estimation. In Proceedings of the 2007 9th International Symposium on Signal Processing and Its Applications, Sharjah, UAE, 12–15 February 2007; pp. 1–4.
14. Gogolev, I.; Yashin, G. Cramér-rao lower bound of Doppler stretch and delay in wideband signal model. In Proceedings of the IEEE Conference of Russian Young Researchers in Electrical and Electronic Engineering (EIConRus), St. Petersburg, Russia, 1–3 February 2017.
15. He, L.; Kassam, S.; Ahmad, F. Sparse Stepped-Frequency Waveform Design for Through-the-Wall Radar Imaging. *IET Digit. Libr.* **2011**, 922–938.
16. Zhu, F.; Zhang, Q.; Lei, Q. Reconstruction of Moving Target's HRRP Using Sparse Frequency-Stepped Chirp Signal. *IEEE Sens. J.* **2011**, *11*, 2327–2334.
17. Zhang, L.; Qiao, Z.; Xing, M. High-Resolution ISAR Imaging With Sparse Stepped-Frequency Waveforms. *IEEE Trans. Geosci. Remote Sens.* **2011**, *49*, 4630–4651. [CrossRef]
18. Axelsson, S. Analysis of Random Step Frequency Radar and Comparison With Experiments. *IEEE Trans. Geosci. Remote Sens.* **2007**, *45*, 890–904. [CrossRef]

19.　Mahdi, S.; Sergiy, A. Cramér-rao Bound for Sparse Signals Fitting the Low-Rank Model with Small Number of Parameters. *IEEE Signal Process. Lett.* **2015**, *22*, 1497–1501.

20.　Yun, S.; Kim, S. Analysis of Cramér-rao Lower Bound for time delay estimation using UWB pulses. In Proceedings of the Ubiquitous Positioning, Indoor Navigation, and Location Based Service, Helsinki, Finland, 3–4 October 2012; pp. 1–5.

21.　Zhou, J.; Zhao, H.; Fu. Q. Performance analysis of one dimensional radar imaging based on sparse and non-uniform frequency samplings. In Proceedings of the IET International Conference on Radar Systems, Glasgow, UK, 22–25 October 2012; pp. 1–7.

22.　Zhao, T.; Huang, T. Cramér-rao Lower Bounds for the Joint Delay-Doppler Estimation of an Extended Target. *IEEE Trans. Signal Process.* **2016**, *64*, 1562–1573. [CrossRef]

23.　Huang, T.; Liu, Y.; Meng, H. Adaptive Compressed Sensing via Minimizing Cramér-rao Bound. *IEEE Signal Process. Lett.* **2014**, *21*, 270–274. [CrossRef]

24.　Benhaim, Z.; Eldar, Y. The Cramér-Rao Bound for Estimating a Sparse Parameter Vector. *IEEE Trans. Signal Process.* **2010**, *58*, 3384–3389. [CrossRef]

25.　Kalouptsidis, N.; Tarokh, V.; Babadi, B. Asymptotic Achievability of the Cramér-Rao Bound for Noisy Compressive Sampling. *IEEE Trans. Signal Process.* **2009**, *57*, 1233–1236.